



Effective disposal of methylene blue using green immobilized silver nanoparticles on graphene oxide and reduced graphene oxide sheets through one-pot synthesis

Eman F. Aboelfetoh · Ali H. Gemeay · Rehab G. El-Sharkawy

Received: 24 October 2019 / Accepted: 3 April 2020 / Published online: 11 May 2020
© Springer Nature Switzerland AG 2020

Abstract This study reveals the feasibility of exploring highly efficient, cost-effective, and stable green adsorbents for the treatment of contaminated water. Here silver nanoparticles (AgNPs) were immobilized onto nanosheets of graphene oxide (GO) through in situ reduction process using green tea aqueous extract. GO reduction to reduced graphene oxide (rGO) and AgNPs decoration on rGO also occurred simultaneously. The impacts of the extract concentration, contact time, and temperature on the synthesis process have been investigated. The synthesized nanocomposites were examined by XRD, FTIR, Raman, SEM, TEM, and TGA. The GO nanosheets were decorated by AgNPs with a crystalline structure and an average particle size of 25 ± 3 nm. The temperature and the extract concentration were considerably affecting the type of the resulting nanocomposites. The GO/Ag nanocomposites were formed at room temperature (27 °C) using different extract concentration (2–18% (v/v)), while the rGO/Ag nanocomposite was formed only at a higher temperature (95 °C) with higher extract concentration (18%). The methylene blue (MB) dye was picked as a water pollutant to explore the

adsorption ability of the nanocomposites. The adsorption behavior of the GO/Ag nanocomposites was examined under diverse factors (MB concentration, adsorbent dosage, pH, and contact time) to achieve optimization. The adsorption data concurs with Langmuir isotherm giving maximum adsorption up to 633 mg g^{-1} . Adsorption kinetics demonstrate good pseudo-second-order compliance. Spontaneous and endothermic nature of adsorption was affirmed via thermodynamic parameters. The nanocomposites could be utilized as eco-friendly and reliable adsorbents in wastewater treatment, as a result of their exceptional productivity and reusing potential.

Keywords Nanocomposites · Green tea · Silver nanoparticles · Dye removal · Adsorption isotherms · Kinetics

Introduction

Metal nanoparticles play a critical role in various applications as they exhibit impressive mechanical, electrical, catalytic, and magnetic properties due to their considerably high surface area and small size relative to the bulk counterparts (Razzaque et al. 2016). Silver nanoparticles (AgNPs) are enormously used in many applications (e.g., medical, cosmetics, catalysis, pharmaceutical, energy, hardware, and water treatment) due to their remarkable chemical, physical, and biological properties (Salem et al. 2015; Aboelfetoh et al. 2017). AgNPs can be

E. F. Aboelfetoh (✉) · A. H. Gemeay · R. G. El-Sharkawy
Chemistry Department, Faculty of Science, Tanta University,
Tanta, Egypte-mail: eman.fahmy@science.tanta.edu.eg
e-mail: efahmy2001@yahoo.com

R. G. El-Sharkawy
Chemistry Department, College of Science, Jouf University,
Aljouf 2014, Sakaka, Saudi Arabia

manufactured using a variety of methods, including chemical reduction, photochemical reduction, electrochemical techniques, microemulsion, microwave, sonochemical, laser ablation, and γ -radiation (Beyene et al. 2017). Notwithstanding the efficiency of these techniques, they relate to certain constraints, such as toxic chemicals, high operating costs, and energy needs. In addition, the presence of a stabilizer is usually necessary in order to avoid excessive accumulation of the nanoparticles formed (Lee and Jun 2019). As a result, there is a growing need to replace these methods with facile, cost-effective, and environmentally friendly systems. Recently, green chemistry has become a focal topic to protect our global environment. Green metal nanoparticle production using natural product extracts is a promising development that would address the obstacles encountered in chemical methods so far (Rolim et al. 2019; Długosz et al. 2020; Ismail 2020). The synthesis assembly of AgNPs using plants has received widespread attention (Hashemi et al. 2020). This is because plant-mediated synthesis is environmentally friendly, readily accessible, inexpensive, yields the highest quantity of nanoparticles, and has a broad variety of metabolites that help to effectively reduce silver ions (Rolim et al. 2019). In addition, the extraction of non-toxic plants for the synthesis of nanoparticles produces natural capping agents (Beyene et al. 2017). Green tea, commonly known as *Camellia sinensis*, is one of the most popular beverages in people's daily lives, on account of its taste, smell and health effects (Lee et al. 2014). It contains various polyphenolic ingredients, the most widely perceived properties of polyphenols are the antioxidant properties that outcome from their capacity to sequester metal particles and to rummage reactive oxygen species (Lee et al. 2014). The use of green tea is therefore known to reduce the risk of various cancers, such as lung, kidney, throat, and stomach cancers (Hou et al. 2013; Fujiki et al. 2018). Recently, tea extract was used to effectively reduce noble metal ions and served as a shielding agent for nanoparticles (Sun et al. 2014; Rolim et al. 2019).

Industrial wastewater contains various contaminants, and synthetic dyes are one of the most substantial pollutants in wastewater for their widespread use (Konicki et al. 2017). Due to their non-degradability, carcinogenicity, and mutagenicity,

eliminating dyes from discharged water are of great concern. Different techniques were connected for the expulsion of these pollutants from contaminated water (Aboubaraka et al. 2017; Kooh et al. 2016; Aboelfetoh et al. 2017). Adsorption is regarded to be the most popular, effective, and economic method used for the expulsion of various contaminants from water (Gemeay et al. 2018b; Aboelfetoh et al. 2018). In water treatment plants, the application of nanomaterials has attracted significant attention because of their large surface areas and more active functionalized sites (Konicki et al. 2017). Currently, there is an incredible concern of graphene oxide due to its accessibility in mass production, easily functionalization in chemical reactions, and high dispersal in water, beside the layered structure with a very large particular surface area (Haldorai et al. 2014; Lightcap et al. 2010). Graphene oxide (GO) nanosheets bear various surface groups, for example, carboxyl, hydroxyl, epoxide, and carbonyl. These groups permit GO nanosheets to be all around scattered in water to yield a colloidal stable solution. (Shao et al. 2015). These particular preferences make it appealing to various applications (Kumar et al. 2013). Considering the superior individual properties of GO and AgNPs, the combination of GO and AgNPs could yield incredible characteristics. Some approaches have been done to synthesize nanocomposites of metallic nanoparticles and GO by depositing metallic NPs on GO nanosheets through physical adsorption (Huang et al. 2010) or by in situ reduction of metallic salts on GO nanosheets (Huang et al. 2016). Unfortunately, various synthesis techniques are heavily dependent on the use of organic solvents, harmful reducing agents, and stabilizers that pose ecological and biological risks (Hebeish et al. 2010). This research focuses on preparing new adsorbents with high adsorption capacity through the eco-friendly approach. We assessed the use of green tea aqueous extract as a productive reductant and safe capping agent in an in situ reduction procedure for synthesizing AgNPs on GO and rGO nanosheets. Synthesized adsorbents are utilized to capture MB, a common pollutant dye, from aqueous solutions. Therefore, the purpose of this work is to recognize the variables that affect the adsorption process and to pick suitable adsorbents with the goal of making it possible to reuse the industrial wastewater effectively.

Experimental

Materials

Graphite powder was obtained from Jodex (England). H_3PO_4 (85%), H_2SO_4 (98%), HCl (37%), H_2O_2 (30%), KMnO_4 , and NaOH were acquired from Fluka. AgNO_3 was collected from Sigma-Aldrich (99%). MB ($\text{C}_{16}\text{H}_{18}\text{ClN}_3\text{S}$), mol. wt. = $319.85 \text{ g mol}^{-1}$ was acquired from Across. All chemicals were utilized as given without purification. Following standard procedures, dilution and standard solutions were rendered using double-distilled water.

Synthesis of GO

Graphene oxide (GO) was prepared as stated before (Huang et al. 2011). Typically, 3 g of graphite is blended with concentrated $\text{H}_2\text{SO}_4/\text{H}_3\text{PO}_4$ (320:80 mL) using a magnetic stirrer. After adding KMnO_4 (18 g) gradually in an ice bath, the mixture was left stirring for 3 days at room temperature. The color of the mixture changed from dim purplish green to dull cocoa. The H_2O_2 solution is added to stop the oxidation reaction, the color of the mixture changed to yellow. To remove any leftover salt, the residue was washed with HCl (20%) and afterward re-dispersed in distilled water. The washing procedure was completed using decantation of the supernatant. The obtained gel was dried at 60°C for 24 h.

Preparation of the green tea extract

Ten grams of dry leaves of green tea was blended with 100 mL of refined water for 30 min at 50°C . The residue was secluded, and the pure extract was acquired by centrifugation at a speed of 6000 rpm. The resultant extract stored at -20°C preceding utilization.

Synthesis of nanocomposites

Scheme 1 summarizes the in situ immobilization of green synthesized AgNPs onto GO and rGO. GO/Ag nanocomposites were created in situ by reducing Ag ions in the presence of GO by including a particular volume of aqueous green tea extract. A typical reaction mixture contains 0.12 g of GO in 50 mL distilled water sonicated for 1 h, accompanied by adding AgNO_3 solution (0.01 M) and a certain volume of aqueous extract, and the

all-out volume was regulated to 100 mL by distilled water. The concentrations of the extract ranged from 2 to 18% (v/v) to maximize AgNP formation. At room temperature, the consequent suspension was disturbed for 2 h. The synthesized samples were purified via centrifugation and washed considerable times utilizing distilled water, ethanol and dried out at 50°C for 48 h. The synthesized materials were assigned in the text as GO/Ag-2, GO/Ag-6, GO/Ag-9, and GO/Ag-18, where the numbers refer to the extract concentrations (%). To assess the impact of temperature and time on the reduction procedure, the mixture of GO and AgNO_3 was refluxed at 95°C for 2 and 24 h with 2% and 18% extract, respectively. The resultant composites were then isolated and washed well with water to expel the excess extract. The obtained samples were named as GO/Ag(2R)-2, GO/Ag(24R)-2, and GO/Ag(24R)-18 where the symbol 2R and 24R denote the reflux time 2 and 24 h, while the number 2 and 18 refers to the extract concentration. Similarly, to study the impact of extract concentration on the reduction of GO, the above experimental procedure was completed by refluxing aqueous solution of GO at 95°C for 24 h using 2 and 18% extract without adding AgNO_3 . The obtained samples were labeled as GO(24R)-2 and GO(24R)-18. The detailed conditions, specific surface areas and the abbreviation symbols of all synthesized materials are listed in Table 1.

Characterization methods

The morphology and the structure of the prepared samples were characterized by SEM (DSM 982 Gemini) and TEM (JEOL-2010). XRD patterns were gathered on MXP-18 diffractometer outfitted with $\text{CuK}\alpha$ radiation. FTIR spectra were recorded using Perkin Elmer 1430. Raman spectrum was conducted on HR Evolution Raman spectrometer (Japan) with excitation laser wavelength of 514 nm. TGA examination was estimated utilizing TGA-50 (Shimadzu) in the presence of N_2 at a heating rate of $15^\circ\text{C}/\text{min}$. The zeta potentials of the synthesized nanocomposite were resolved at various pH using Malvern Zetasizer 2000. The concentration of MB color was measured using the spectrophotometric method utilizing Cary 400 UV–visible spectrophotometer ($\lambda_{\text{max}} = 665 \text{ nm}$).

Scheme 1 In situ immobilization of green synthesized AgNPs onto GO and rGO (a) and the proposed adsorption mechanism of MB (b)

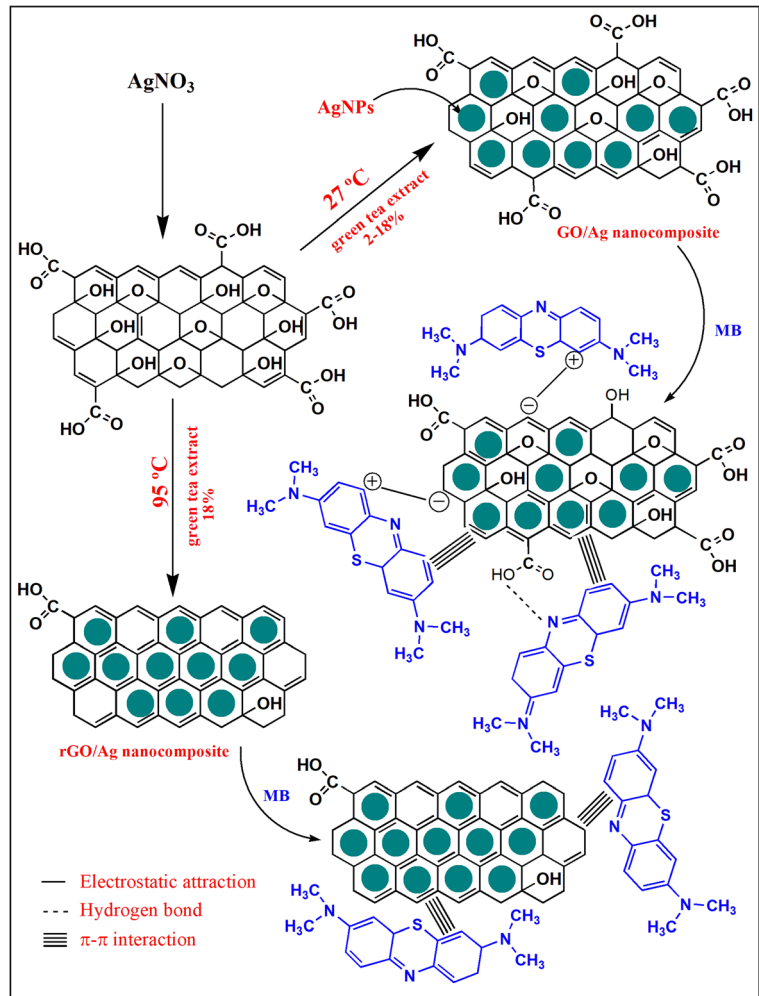


Table 1 Synthesis conditions of the prepared samples and their calculated specific surface areas

Sample name	Green tea extract conc. (v/v) %	Stirring time (h)	Temperature ($^\circ\text{C}$)	$[\text{AgNO}_3]$ (mol L^{-1})	Specific surface area ($\text{m}^2 \text{g}^{-1}$)
GO/Ag-2	02.0	2	27	0.01	1201.34
GO/Ag-6	06.0	2	27	0.01	1328.55
GO/Ag-9	09.0	2	27	0.01	1430.34
GO/Ag-18	18.1	2	27	0.01	1107.12
GO/Ag(2R)-2	02.0	2	95 (reflux)	0.01	—
GO/Ag(24R)-2	02.0	24	95 (reflux)	0.01	1129.28
GO/Ag(24R)-18	18.1	24	95 (reflux)	0.01	678.47
GO(24R)-2	02.0	24	95 (reflux)	—	973.44
GO(24R)-18	18.1	24	95 (reflux)	—	632.44
GO	—	—	—	—	1060.34

Batch adsorption experiments

Adsorption examinations were done with varying initial concentrations of MB aqueous solutions (9.5–28.7 mg L⁻¹). For every run, a certain weight (1.1–2.8 mg) of the prepared adsorbents was mixed with distilled water (10 mL) and sonicated for 2 min., then 1.5 mL of MB solution was added, and the total volume kept at 25 mL by distilled water. The solution pH was set to optimum values using phosphate buffer with drops of NaOH (0.1 M) or HCl (0.1 M). The mixture continued shaking, and the color concentration was evaluated at time intervals employ UV-vis spectrophotometer. The adsorption capabilities at equilibrium (q_e) were resolute by the accompanying Eq. (1):

$$q_e = (C_o - C_e) \frac{V}{m} \tag{1}$$

where C_o and C_e are abbreviations for the initial and equilibrium concentrations of MB (mg L⁻¹). The adsorption rate for MB color, i.e., the MB removal effectiveness was determined using the following Eq. (2):

$$\text{Removal (\%)} = \frac{C_o - C_t}{C_o} \times 100 \tag{2}$$

where C_t refers to the final concentration of MB (mg L⁻¹) at different times of adsorption process.

Results and discussion

Characterization of adsorbents

XRD

The XRD of GO and GO/Ag nanocomposites (GO/Ag-2, GO/Ag-6, GO/Ag-9, and GO/Ag-18) displayed a strong peak at $2\theta = 10.7^\circ$ (d-spacing = 0.84 nm) indicating the presence of GO (Fig. 1a). By increasing the extract concentration, the intensity of this peak decreased and new peaks at $2\theta = 38.1^\circ, 44.4^\circ, 64.4^\circ,$ and 77.6° appeared. These peaks are characteristic for AgNPs (Kumar et al. 2013) and their intensities were increased in this way GO/Ag-2 < GO/Ag-6 < GO/Ag-9 < GO/Ag-18 (Fig. 1a). The mean crystallite size of the AgNPs was calculated by Scherer’s equation (Agnihotri et al. 2014) and found to be ~ 25–28 nm. At low extract

concentration (2%), with a rise in the synthesis temperature to 95 °C and time from 2 to 24 h, the intensity of AgNPs has been increased along this direction, GO/Ag-2 < GO/Ag(2R)-2 > GO/Ag(24R)-2 (Fig. 1b), and the characteristic peak of GO with lower intensity is still present. This may be indicated that the low extract concentration (2%) was not enough to reduce GO to rGO. Through rising the extract concentration to 18% as for GO/Ag(24R)-18, the intensity of AgNPs increased further and the characteristic peak for GO completely vanished which affirms the reduction of GO to rGO. The absence of the distinctive peak of rGO may be due to the decoration of AgNPs and the disorder of the decorated rGO sheets (Tang et al. 2013).

The influence of extract concentration and temperature on the reduction of GO was also investigated (Fig. 2a). By refluxing the GO solution with 2% aqueous extract at 95 °C for 2 h (GO(24R)-2), the intensity of the characteristic peak of GO was decreased and a new small broad peak at $2\theta = 25.56^\circ$ corresponding to rGO emerged (Xiong et al. 2010). It may be due to the low concentration of the extract, which is not adequate to reduce GO altogether. Through increasing the extract concentration to 18% at the same synthesis temperature (95 °C) for 24 h as for GO(24R)-18, the characteristic peak for GO entirely disappeared and only a significant broad peak for rGO appeared at $2\theta = 25.56^\circ$.

Raman

Raman scattering is firmly sensitive to the electronic structure and has turned out to be a basic tool for portraying crystal structure, disorder, and deformities in carbon-containing materials. For instance, the GO reduction can appear in Raman spectra through the adjustments in the band positions, and the relative intensity of principle peaks, D and G (Sobon et al. 2012). This information has been used to validate the reduction of GO to rGO for sample GO/Ag(24R)-18, throughout the in situ immobilization of AgNPs on the GO. Figure 2b demonstrates the Raman spectrum of the GO/Ag(24R)-18 nanocomposite. The spectrum displays two noticeable bands at approximately 1342 cm⁻¹ and 1586 cm⁻¹. Such bands were allocated to the D and G bands of rGO in that sample (Dubale et al. 2014; Sang et al. 2017). In addition, the calculated D/G intensity ratio for the GO/Ag(24R)-18 (I_D/I_G) was 1.19. This finding is quite close to a previous study published for other rGO/Ag nanocomposite (Sang et al. 2017)

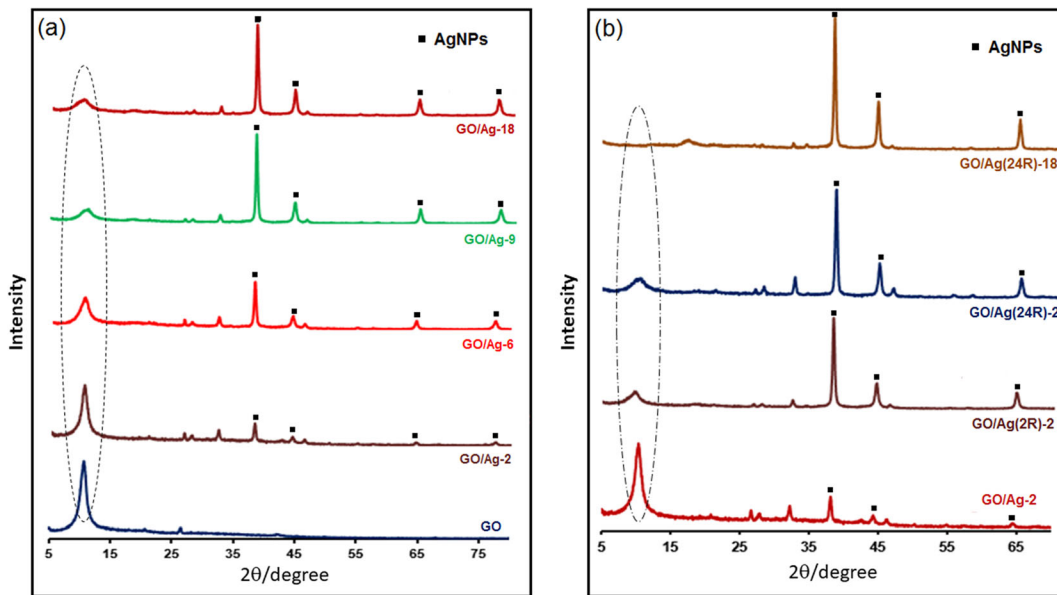


Fig. 1 XRD peaks of GO and GO/Ag nanocomposites that formed at a 27 °C with different extract concentrations (%) and b 95 °C with 2 and 18% extract after 2 and 24 h

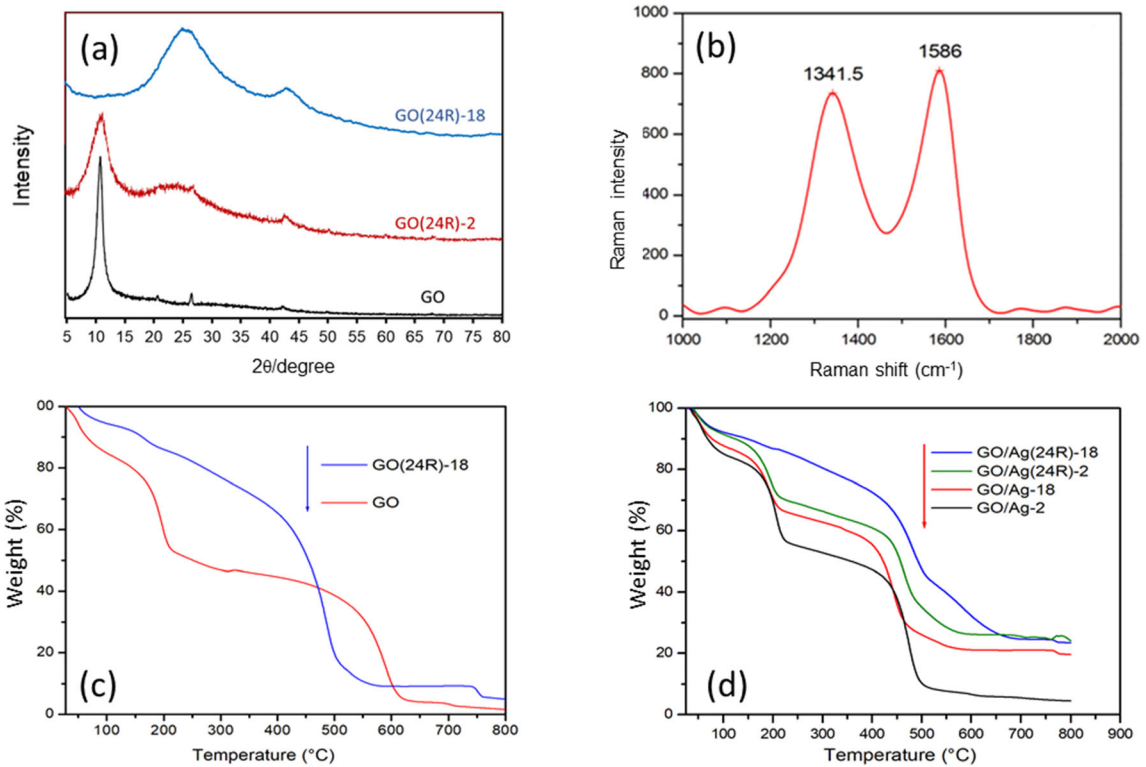


Fig. 2 XRD peaks of GO, GO(24R)-2, and GO(24R)-18 (a), Raman spectrum of GO/Ag(24R)-18 (b), and TGA examination of GO, GO(24R)-18, (GO/Ag-2, GO/Ag-18, GO/Ag(24R)-2, and GO/Ag(24R)-18 (c and d)

confirming the reduction of GO to rGO in our nanocomposite, GO/Ag(24R)-18.

TGA

The thermal behavior of GO, rGO (GO(24R)-18), and their composites with AgNPs (GO/Ag-2, GO/Ag-18, GO/Ag(24R)-2, and GO/Ag(24R)-18) were examined (Fig. 2c, d). In Fig. 2c, the TGA curve of GO clearly shows three steps of weight loss. The first weight loss happened below 100 °C because of the vaporization of dampness from GO. The second weight loss of about 28 wt.% was at a temperature range (150–230 °C). The enormous weight reduction in this temperature range was connected with “the expulsion of oxygen-containing functional groups” (Chook et al. 2012; Konicki et al. 2017). Additionally, GO showed further weight reduction between 450 and 620 °C, basically because of the decomposition of the graphitic carbons (de Moraes et al. 2015). The GO(24R)-18 sample shows just a lesser weight reduction (6 wt.%) between 130 and 200 °C. This recognition may demonstrate that an enormous bit of the oxygen functionalities was adequately removed during the reduction procedure. For GO/Ag nanocomposites (Fig. 2d), the weight loss in the range of 150–230 °C decrease from the GO/Ag-2, GO/Ag-18, and GO/Ag(24R)-2 to be 25.5, 18.4, and 17.5 wt.%, respectively. This indicates that by increasing the extract concentration and the synthesis temperature (95 °C), the fraction of oxygenic groups is reduced. In addition, the GO/Ag(24R)-18 sample showed very small weight loss (4 wt.%) in the range of 150–230 °C which is comparable with the rGO sample (GO(24R)-18). This could support the complete reduction of the oxygenic groups by high extract concentration (18%) at 95 °C and the formation of rGO/Ag nanocomposite. The findings of TGA align well with those of XRD analysis. Moreover, the high thermal stability of the nanocomposites may also be due to the existence of AgNPs.

FTIR

The FTIR spectrum of GO (Fig. 3a) showed multiple bands at 3400 cm^{-1} , 1630 cm^{-1} , 1730 cm^{-1} , 1050 cm^{-1} , and 1223 cm^{-1} , allocated for –OH stretching, C=C stretching, C=O of the carboxyl group, and C–O stretching of alkoxy and epoxy species, respectively (Aboelfetoh et al. 2018), affirming the effective oxidation of graphite. When AgNPs were immobilized on GO

nanosheets at room temperature, GO/Ag nanocomposites (Fig. 3a) displayed spectra entirely like that for GO with lower intensities and the carboxylic group’s C=O vibration at 1730 cm^{-1} was diminished by rising the extract concentrations. This may mirror the connection between the carboxylic groups of GO nanosheets and AgNPs by shaping a chemical bond or electrostatic attraction, which was reliable with a comparative previous study (Shao et al. 2015). The significant shift of bands and the appearance of small bands at 2920 and 2852 cm^{-1} , especially at higher extract concentrations, may confirm the effective recombination of the functional groups of green tea extract with GO/Ag nanocomposites, thereby improving the stability of nanocomposites (Liu et al. 2017). These results are consistent with previous reports showing the existence of green tea polyphenols as a stabilizer for the AgNPs surface (Rolim et al. 2019; Rónavári et al. 2017).

With respect to the green reduction of GO in presence of 2% extract at high temperature, FTIR of GO(24R)-2 showed a pronounced rebate in the intensity of OH band (3400 cm^{-1}) and significantly changed the locations of the characteristic GO bands (Fig. 3b). This is attributable to the partial reduction of GO to rGO. Through increasing the extract concentration to 18% as with GO(24R)-18, the carboxyl group’s vibration band (1730 cm^{-1}) disappeared completely and a new band emerged at 1586 cm^{-1} . This can be ascribed to the skeletal vibration of C–C of rGO sheets (Hou et al. 2011), indicating a complete reduction of GO. In addition, GO/Ag(24R)-18 nanocomposite showed very close spectra (not shown) to that for GO(24R)-18 supporting the reduction of GO to rGO in that sample.

SEM and TEM

SEM was utilized to describe the morphology of nanocomposites. As shown in Fig. 4, the SEM image of GO (Fig. 4a) exhibits a layered structure. SEM clearly confirm the presence of spherical AgNPs on the surface of GO/Ag-9 nanocomposite at low and high magnifications (Fig. 4b, c). Nonetheless, the GO/Ag-2, synthesized with low extract concentration (2%) at room temperature hardly show the AgNPs with a smaller size on its surface (Fig. 4d). At the same extract concentration (2%) by raising the temperature to 95 °C for 24 h, as for GO/Ag (24R)-2, the presence of AgNPs was significant with larger particle size than that synthesized at room temperature (GO/Ag-2) (Fig. 4e). To validate the

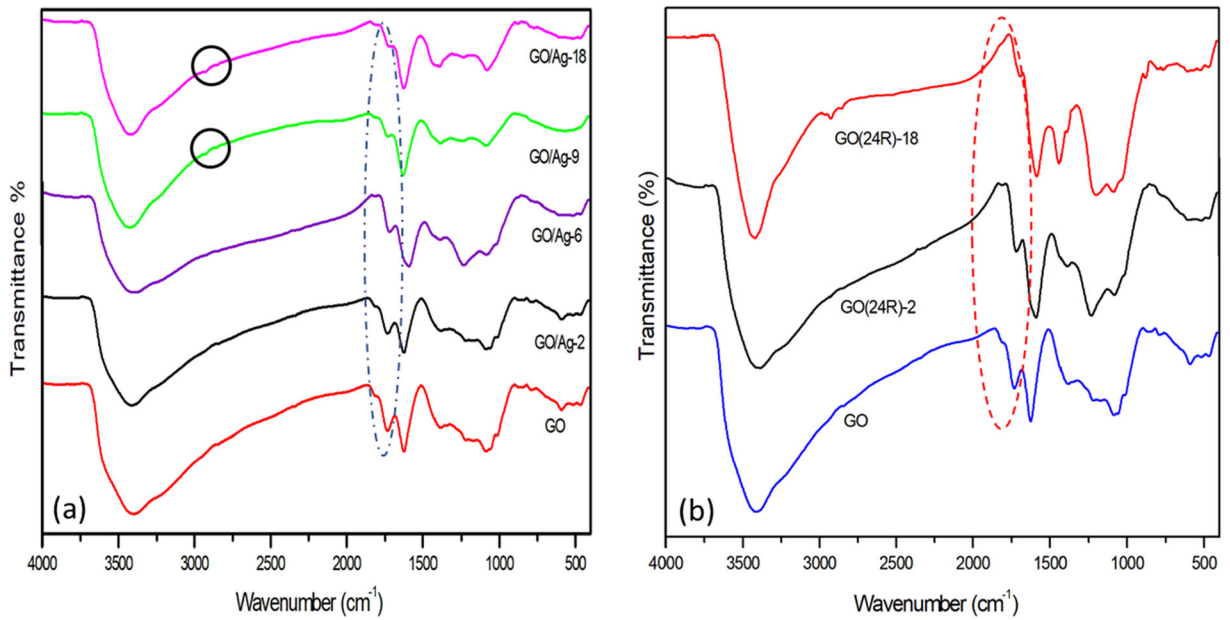
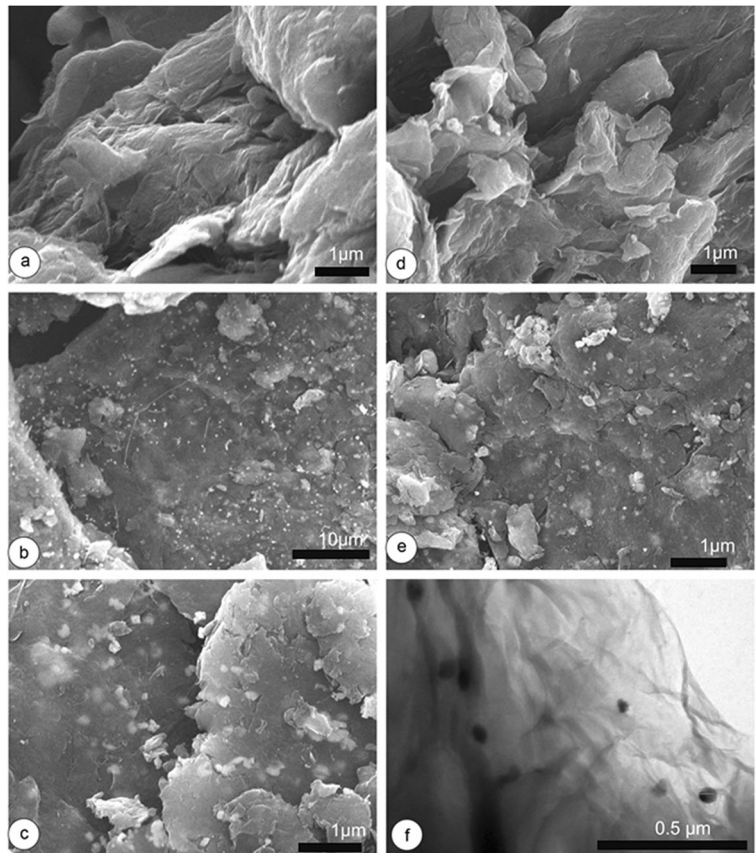


Fig. 3 FTIR spectra of **a** GO, and GO/Ag nanocomposites synthesized at 27 °C using different extract concentrations (%) and **b** GO, GO(24R)-2 and GO(24R)-18

Fig. 4 SEM images of GO (a), GO/Ag-9 at low magnification (b), GO/Ag-9 at high magnification (c), GO/Ag-2 (d), GO/Ag (24R)-2 (e), and TEM of GO/Ag-9 (f)



morphology seen in the SEM images, TEM was used to visualize the structure of the nanocomposites. From Fig. 4f, It can be seen that GO has a crumpled structure and that spherical AgNPs of 15–40 nm size were uniformly distributed over the GO surface. These particles averaged 25 ± 3 nm in diameter, which is compatible with the size of XRD. Moreover, the particle size of AgNPs increases with some agglomeration, especially for nanocomposites that are prepared at a high temperature with high extract concentration.

Effect of synthesis factors on the removal of MB

To explore highly effective adsorbents for MB elimination, the impact of the preparation factors was examined. Table 1 shows the abbreviation symbols of the synthesized samples.

Effect of extract concentration

The effect of GO/Ag nanocomposites prepared by different green tea extract concentrations (2–18%) at room temperature on the MB removal rate was investigated (Fig. 5a). It is probable that the green tea extract could control not only AgNP growth rate but also the MB removal rate. Increasing the extract concentration from 2 to 9% raises the removal percentage as per the next order $GO/Ag-2 < GO/Ag-6 < GO/Ag-9$. This may be indicative of the increase in AgNPs yield in that direction. This behavior is very much in line with the XRD results which evidently reveal the growth of AgNP

peaks as the extract concentration increased. Increasing the extract concentration further (18%) as with the GO/Ag-18, the removal efficacy decreases to 78% within 10 min. That may be due to aggregates of AgNPs with smaller surfaces (Allen et al. 2010). The calculated specific surface areas of the prepared nanocomposites (Table 1) confirmed the above aspect.

It is interesting to state that the GO/Ag nanocomposites showed removal effectiveness better than those for GO. This may confirm the main role of AgNPs in the adsorption process, where they considered being additional adsorption sites for MB dye alongside the available adsorption sites on the GO surface. Furthermore, the presence of AgNPs affects the characteristics of GO and improves the separation of prepared GO/Ag nanocomposites from the medium of reaction compared with GO. This was agreed with previous research that AgNPs had large areas to help adsorb organic colors on their surfaces (Vidhu and Philip 2014; Gemeay et al. 2018a). It was evident from Table 1 that the nanocomposites being prepared (GO/Ag-2, GO/Ag-6, and GO/Ag-9) had greater surface areas than those calculated for GO.

Effect of synthesis temperature and stirring time

Temperature and contact time were found to impact the removal effectiveness of the nanocomposites (Fig. 5b). The nanocomposites synthesized after 2 and 24 h in the presence of 2% extract at high temperature (95 °C) such as GO/Ag(2R)-2 and GO/Ag(24R)-2 showed lower removal efficacy for MB than those produced at room

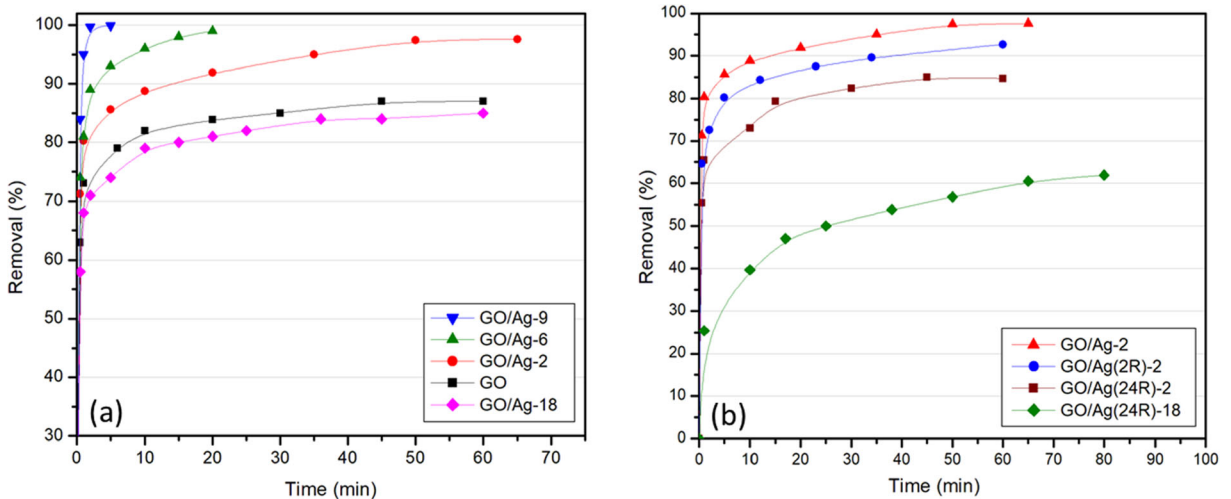


Fig. 5 Removal efficacy of MB (22.10 mg L^{-1}) in the existence of GO/Ag nanocomposites (2.3 mg) that formed at a 27 °C with varying extract concentrations (%) and b 95 °C with 2 and 18% extract after 2 and 24 h

temperature after 2 h (GO/Ag-2), where the adsorption efficiency declines in this order, GO/Ag(24R)-2 < GO/Ag(2R)-2 < GO/Ag-2. This can be due to the higher temperature (95 °C) and the longer stirring time (24 h) that accelerates the production of more AgNPs with larger size as shown by SEM. Therefore, the surface exposed to adsorption may be reduced. Moreover, the GO/Ag(24R)-18, synthesized under these conditions (18% extract, 95 °C, 24 h) showed much lower performance than other nanocomposites. This may be due to the presence of the AgNP clusters and the reduction of GO to rGO as affirmed by Raman and TGA. Increasing the surface coverage of green tea biomolecules could also hinder the diffusion of MB on the GO/Ag(24R)-18 surface. Besides that, GO(24R)-18, which synthesized at 95 °C in the presence of 18% extract displayed lower removal effectiveness for MB than GO (Fig. 6a). This could be due to the reduction of GO to rGO. While GO(24R)-2 showed superior removal efficiency to that reported for GO(24R)-18 (Fig. 6a), where GO is still present with only partial reduction of GO to rGO in that sample.

Effect of kinetic variables for the removal of MB

Effect of adsorbent dosage

The impact of the adsorbent doses on the elimination effectiveness of MB by the selected nanocomposite, GO/Ag-2, was appeared in Fig. 6b. It was found that the increase in GO/Ag-2 dosage from 1.1 to 2.8 mg enhances the adsorption of MB from 61.2 to 98.6% within 5 min. This was due to an increase in adsorption sites.

Effect of MB concentration

The adsorption ability of the selected nanocomposite (GO/Ag-6) at various MB concentrations appeared in Fig. 7. It was noticed that adsorption ability increased from ~225 to 507 mg g⁻¹ when the MB concentration increased from 9.5 to 28.7 mg L⁻¹, respectively. During the initial 10 min, there was rapid adsorption that could be ascribed to the availability of active adsorbent sites. After that, the adsorption rate reduced bit by bit as the equilibrium reached. The short equilibrium time mirrors the effectiveness of the synthesized adsorbents and their appropriateness for fast and quantitative removal of the dye. Adsorption bends were smooth and continued until

saturation state showing the conceivable plan of monolayer inclusion on the adsorbent surface by dye molecules (Ghaedi et al. 2012).

Effect of pH

The solutions pH mirrors a momentous effect on the adsorption capacity of various adsorbents because of the separation of diverse functional assemblies on the adsorbent active sites and ionization of adsorbate materials in solution (Chieng et al. 2015). MB adsorption analyses using the selected nanocomposite (GO/Ag-6) were performed within pH range 2–9 (Fig. 8a). It was found that the adsorption efficiency increased with increasing pH. The zeta potential values of the GO/Ag-6 in water were measured at the same pH range (2–9) (Fig. 8b) to investigate the magnitude and sign of the surface charge density around the particles. It was negatively charged over the entire pH range studied and the negative charges enhanced with increasing pH. This could be due to the ionization of functional groups (carboxylic and/or hydroxyl) on the GO nanosheets. In accordance with a previous study, the results indicated that when AgNPs were immobilized on GO nanosheets, GO/Ag nanocomposite had greater negative charge than that recorded for GO at the same pH range, indicating that GO-Ag nanocomposite was more stable than GO (Vi et al. 2018). This due to the synergistic effects of GO and biosynthesized AgNPs (Liu et al. 2017). Hence, at high pH, the selected adsorbent (GO/Ag-6) gains its higher negative charges. This increases the surface charge density and consequently increases the adsorption of MB because of increasing electrostatic attraction between negatively charged nanocomposite and positively charged dye (Scheme 1).

It has been reported that the coexistence of oxygen-containing functional groups and aromatic sp² domains allow GO nanosheets to participate in a wide variety of bonding and interactions (Martínez-Orozco et al. 2013; Konicki et al. 2017). Accordingly, a plausible mechanism for MB adsorption procedure on the synthesized GO/Ag nanocomposites has been deduced as shown in Scheme 1. The disposal way of MB by GO/Ag nanocomposites could be via electrostatic interactions and hydrogen bonding between carboxyl or hydroxyl surface groups of GO with N atoms in dye molecules (Heidarizad and Şengör 2016; Haque et al. 2019). Also, the aromatic rings of the dye can interact with π electrons of GO through π - π electron coupling. This may

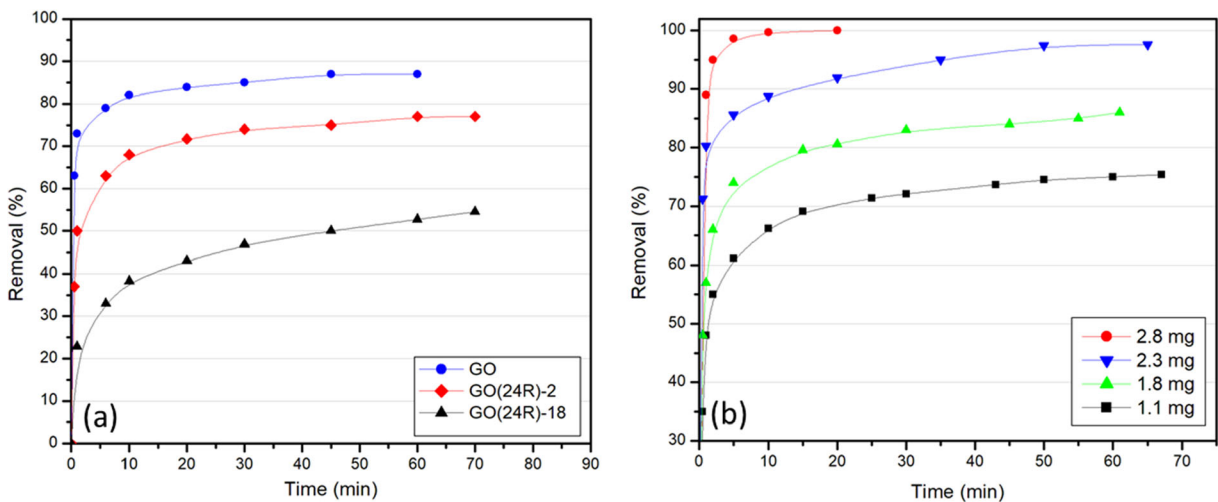


Fig. 6 Removal efficacy of MB (22.10 mg L^{-1}) in the presence of **a** 2.3 mg of GO, GO(24R)-2, and GO(24R)-18 and **b** different amounts of GO/Ag-2

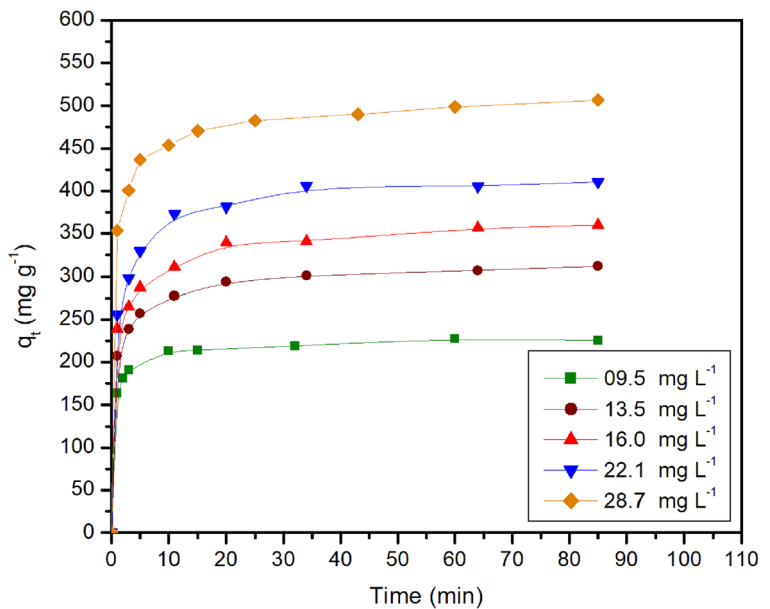
explain the high efficiency of these substances in removing the dye (Fig. 5a). While the removal of MB by rGO/Ag nanocomposite (GO/Ag(24R)-18) may occur primarily through π - π interaction due to the removal of most of the oxygen-containing groups. This would elucidate the low removal efficacy of this sample compared with the GO/Ag nanocomposites (Fig. 5b).

Regeneration and reuse study

The economic viability of using adsorbent materials to exclude dyes from water solutions depends on their

potential for reuse and regeneration. The reuse potential of the selected sample (GO/Ag-6) was studied for successive adsorption/desorption cycles. The effective desorption of MB dye from the spent adsorbent (GO/Ag-6) was made by separating the adsorbent from the suspension by centrifugation, followed by washing with 0.1 M NaOH, diluted ethanol, and distilled water. Before further processing, the washed sample has been dried. The adsorption efficiency of GO/Ag-6 was not compromised after 4 cycles (Fig. 9). This shows that the synthesized nanocomposites (GO/Ag) are remarkably reusable adsorbents for expelling MB from water solutions.

Fig. 7 The adsorption capacity of GO/Ag-6 (1.10 mg) at assorted initial concentrations of MB



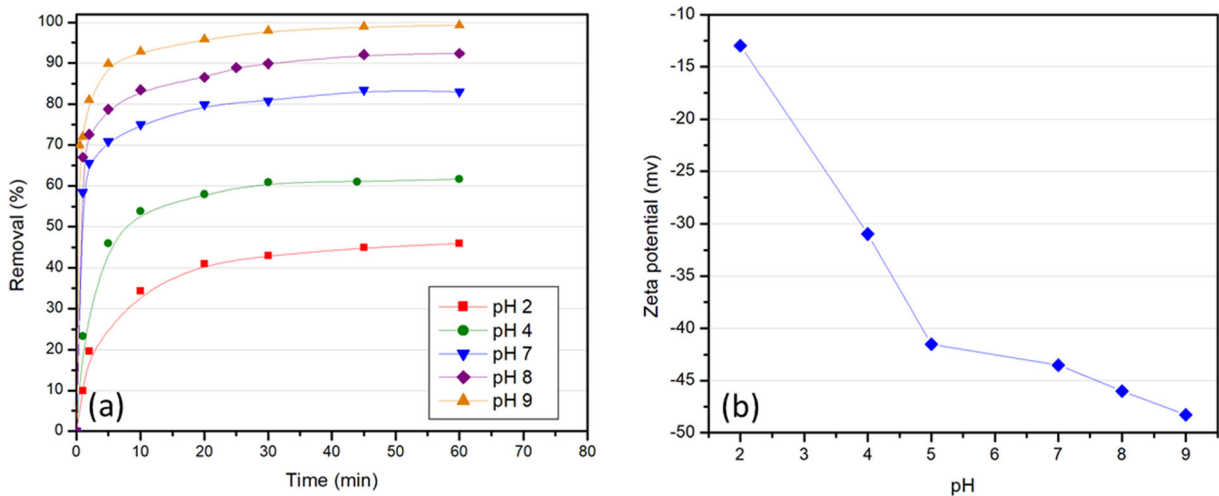


Fig. 8 a Removal efficacy of MB (22.10 mg L^{-1}) in the presence of GO/Ag-6 (1.1 mg) at various pH and b zeta potential of GO/Ag-6 at the same pH ranges

Modeling of adsorption kinetics

The MB adsorption kinetics from aqueous solution to the nanocomposite surface was inspected utilizing assorted kinetic models “pseudo-1st-order, pseudo-2nd-order, and intraparticle diffusion”. The pseudo-1st-order model represented by the following Eq. (3):

$$\ln(q_e - q_t) = \ln(q_e) - K_1 t \quad (3)$$

The following symbols, q_t (mg g^{-1}) and q_e (mg g^{-1}), denote the adsorption capacity of MB at any time t and at equilibrium, whereas k_1 (min^{-1}) alludes to the rate constant “pseudo-1st-order model”. The equation of the pseudo-2nd-order was formulated as follows (4):

$$\frac{t}{q_t} = \frac{1}{k_2 q_e^2} + \frac{t}{q_e} \quad (4)$$

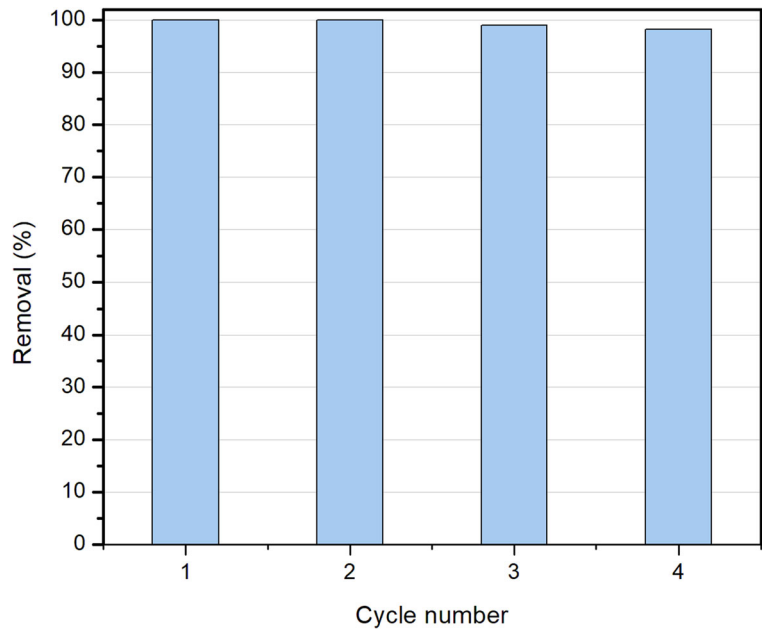
where k_2 ($\text{g mg}^{-1} \text{ min}^{-1}$) is an abbreviation for the rate constant “pseudo-2nd-order model”. The rate constant for every adsorption model was computed and outlined in Table 2. From this table, it appears that the kinetic information fits perfectly with the pseudo-2nd-order equation (Fig. 10a), as shown by the higher correlation coefficients (R^2). In addition, the calculated q_e values for “the pseudo-2nd-order” were deeply matched to the experimental data. For more information about the adsorption mechanism and the rate dominant steps, the data were additionally examined utilizing the intra-

particle diffusion model (Aboelfetoh et al. 2018). This model was labeled by the subsequent equation (5):

$$q_t = K_p t^{0.5} + C \quad (5)$$

where K_p refers to the intra-particle diffusion rate ($\text{mg g}^{-1} \text{ min}^{-0.5}$) and C is a constant which affords data about the boundary layer thickness. Figure 10b demonstrates the plots of q_t versus $t^{0.5}$ of the adsorption data for various concentrations of MB. The plots offer two linear segments far from reaching the origin point which illustrate that intraparticle diffusion is not the rate-limiting stage. The two intersecting sections show that adsorption takes place in two stages. The first section depicts the outer surface diffusion while the other one describes the diffusion through the inner surface. According to the fact shown in Table 2, the external diffusion over the adsorbent surface (GO/Ag-6) is a very fast step followed by a fully slow diffusion into the internal surface (Gao et al. 2013; Yang et al. 2016). It has been found that $k_{p1} > k_{p2}$ and increases with increased concentration of MB. This proposed that the adsorption process was ruled by the outer mass transport of MB particles. According to SEM and TEM results, the synthesized nanocomposites were in a form of thin sheets. In this way, the MB molecules can be accessed and adsorbed promptly on the functional surface groups in line with a previous study (Li et al. 2013b).

Fig. 9 Removal efficacy of MB (22.10 mg L⁻¹) on GO/Ag-6 (2.8 mg) after 4 cycles



Thermodynamic study

To get more information about the energy changes related to the adsorption process, the thermodynamic parameters “ ΔG° , ΔH° , and ΔS° ” for MB adsorption on selected adsorbents were assessed using these equations (6 and 7).

$$\Delta G^\circ = RT \ln (q_e/C_e) \tag{6}$$

$$\ln (q_e/C_e) = \Delta S^\circ /R - \Delta H^\circ /RT \tag{7}$$

where q_e/C_e , R (8.314 J mol⁻¹ k⁻¹), and T (in kelvin) refer to the distribution coefficient, gas constant, and the absolute temperature separately. The calculated values of these parameters (ΔG° , ΔH° , and ΔS°) were recorded in Table 3. The negative estimations of ΔG° demonstrates the spontaneity and feasibility of the adsorption process. The values of ΔG° for GO/Ag nanocomposites such as GO/Ag-9 and GO/Ag-2 were more negative

Table 2 Parameters of kinetic models at different initial MB concentration for the adsorption of MB onto GO/Ag-6

MB (mg L ⁻¹)	Pseudo-first-order model				Pseudo-second-order model		
	$q_e, \text{exp (mg g}^{-1}\text{)}$	$q_e, \text{cal (mg g}^{-1}\text{)}$	$K_1 \text{ (min}^{-1}\text{)}$	R^2	$q_e, \text{cal (mg g}^{-1}\text{)}$	$K_2 \text{ (g mg}^{-1} \text{min}^{-1}\text{)}$	R^2
09.5	226	23.5	0.041	0.8402	227	0.0071	0.9999
13.5	318	37.0	0.038	0.7519	320	0.0027	0.9998
16.0	347	55.4	0.057	0.8233	349	0.0024	0.9998
22.1	392	43.5	0.042	0.7565	394	0.0025	0.9999
28.7	508	49.0	0.035	0.7044	510	0.0021	0.9999
MB (mg L ⁻¹)	Intra-particle diffusion model						
	$K_{p1} \text{ (mg g}^{-1} \text{min}^{-0.5}\text{)}$		$C_1 \text{ (mg g}^{-1}\text{)}$	R^2	$K_{p2} \text{ (mg g}^{-1} \text{min}^{-0.5}\text{)}$	$C_2 \text{ (mg g}^{-1}\text{)}$	R^2
09.5	33.50		84.64	0.9680	1.809	207.93	0.9061
13.5	40.14		137.32	0.9880	5.325	266.87	0.9372
16.0	54.72		166.47	0.9961	6.148	287.12	0.9161
22.1	72.43		128.55	0.9902	5.844	335.89	0.9460
28.7	97.76		263.90	0.9904	6.605	437.90	0.9762

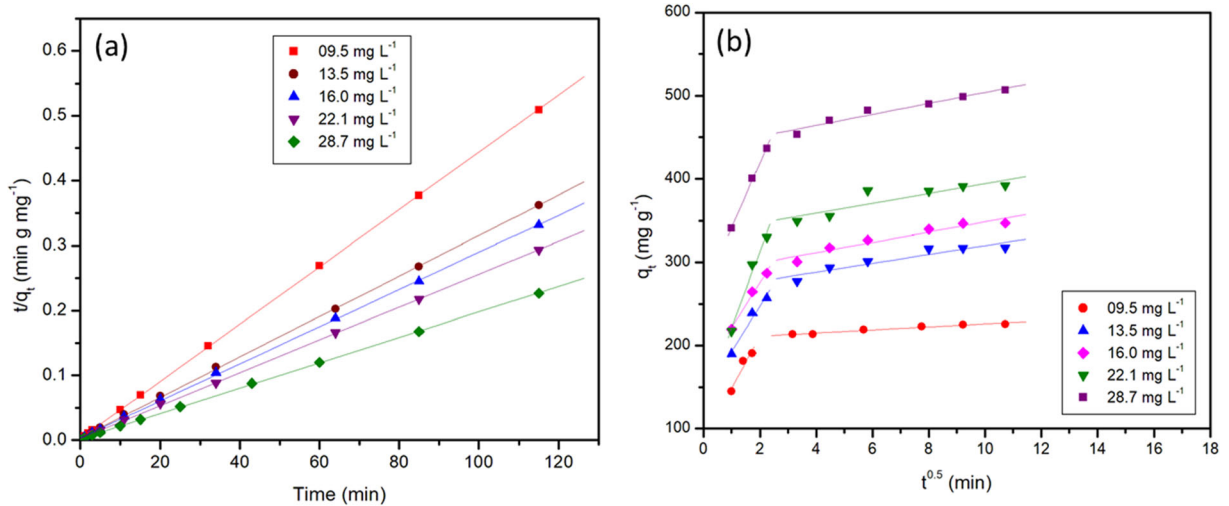


Fig. 10 The pseudo-2nd-order plot (a) and the particle diffusion plot for MB adsorption on GO/Ag-6 (b)

than those of rGO/Ag nanocomposite (GO/Ag(24R)-18) and reduced graphene oxide (GO(24R)-18), suggesting more favorable adsorption of GO/Ag nanocomposites. In addition, with the increase in temperature these values become more negative, suggesting that the adsorption process is more desirable with temperature. The positive values of ΔH° for all adsorbents demonstrate the heat-absorbing nature of adsorption (Sharma et al. 2013). The positive ΔS° values indicate the increased randomness at the interface of solid/solution.

Adsorption isotherms

The adsorption isotherm indicates how retained particles diffuse between the liquid phase and the solid surface when equilibrium is accomplished during adsorption. The examination of the isotherm information by fitting them to various isotherm models is a vital step in finding an appropriate model. The adsorption limit of the synthesized nanocomposites was explored with Freundlich, Langmuir, and Temkin adsorption isotherms. The Langmuir isotherm model expects a monolayer scope of adsorbent, and the adsorption happens over particular homogeneous active sites on the adsorbent surface (Aboelfetoh et al. 2018). The linear equation of the Langmuir model was depicted with the subsequent relation (8):

$$\frac{C_e}{q_e} = \frac{C_e}{q_{max}} + \frac{1}{q_{max} K_L} \tag{8}$$

where C_e (mg L^{-1}) is the dye concentration at equilibrium, q_{max} is the monolayer adsorption limit (mg g^{-1}), and K_L is a Langmuir constant (L mg^{-1}). Based on the Freundlich isotherm model, the adsorption happens on heterogeneous surfaces with the connection between the adsorbed molecules and is not limited to the development of a monolayer (Aboelfetoh et al. 2018). The Freundlich model was given by the accompanying relation (9):

$$\ln q_e = \ln K_F + \frac{1}{n} \ln C_e \tag{9}$$

where K_F and n refer to Freundlich constants “which symbolize adsorption capacity and adsorption strength respectively”. The Temkin isotherm model expects that the adsorption heat would diminish directly with expanding coverage because of the interactions between adsorbate and adsorbent (Mahmoud et al. 2017). This model was represented by the following equation (10):

$$q_e = B \ln K_T + B \ln C_e \tag{10}$$

where K_T is the Temkin constant (L mg^{-1}) equivalent to the maximum binding energy and B (J mol^{-1}) is a constant linked to the heat of adsorption. The Dubinin-Radushkevich (D-R) model, another adsorption model, was also used for estimating the mechanism of surface adsorption using the following equations (11–13):

Table 3 Thermodynamic parameters for the adsorption of MB on the selected adsorbent samples

Adsorbents	T (°C)	ΔG° (kJ mol ⁻¹)	ΔH° (kJ mol ⁻¹)	ΔS° (J mol ⁻¹ K ⁻¹)
GO/Ag-2	27	-28.90	11.30	134
	35	-29.97		
	45	-31.31		
GO/Ag-9	27	-30.04	08.36	128
	35	-31.06		
	45	-32.34		
GO/Ag(24R)-18	27	-19.90	27.80	159
	35	-21.01		
	45	-22.76		
GO(24R)-2	27	-24.90	17.4	141
	35	-26.02		
	45	-27.43		
GO(24R)-18	27	-18.50	31.9	168
	35	-19.84		
	45	-21.52		

$$\ln q_e = -\beta \varepsilon^2 + \ln q_s \tag{11}$$

$$\varepsilon = RT \ln (1/C_e + 1) \tag{12}$$

$$E = \frac{1}{\sqrt{2\beta}} \tag{13}$$

In light of the D-R model, the hypothetical saturation capacity of MB symbolized by the q_s (mg g⁻¹). A constant “relating to the mean free energy of adsorption” and Polanyi potential by symbols β (mol² k⁻¹ J⁻²) and ε (J mol⁻¹) were also denoted, respectively. In this manner, the plot of $\ln q_e$ vs ε^2 affords a straight line with an inclination (β) and an intercept (q_s) (Aboelfetoh et al. 2018). The mean energy of adsorption (E) determined from Eq. (13) gives data about the nature of adsorption (Shao et al. 2014). Contingent upon the E value, the sort of adsorption can be determined. It can be physical when E is between 1 and 8 kJ mol⁻¹ and can be chemical when E is more than 8 kJ mol⁻¹ (Shao et al. 2014; Aboelfetoh et al. 2018). The constants and R^2 values acquired for all isotherm models are shown in Table 4. Due to the high correlation coefficients for the Langmuir model, the adsorption information corresponds to this model. Additionally, the adsorption strength (n) disclosed a worth more than one reflecting propitious adsorption (Gemeay et al. 2018a). From the results of

the D-R model (Table 4), the MB removal over the synthesized adsorbents is achieved by physical process according to the low values of E (< 8 kJ mol⁻¹). Thus, the removal of MB occurred through the physical adsorption process incorporating a monolayer.

Methylene blue (MB) has been commonly used for assessing the specific surface area of different solids, for example, clays, silicates, and activated carbons in an aqueous medium (Ahmadzadeh Tofighy and Mohammadi 2014; Hegyesi et al. 2017; Ferrero 2010). Because the Langmuir model well defined the adsorption process of MB, the adsorption ability for complete monolayer coverage (q_{max}) can be used to determine the area available for solids, given that the area occupied by an adsorbed MB molecule is identified (Ahmadzadeh Tofighy and Mohammadi 2014). According to this approach, q_{max} was used to estimate the specific surface areas of the as-prepared adsorbents towards MB by Eq. (14) and their values were listed in Table 1.

$$S = \frac{q_{max} N_A a_{MB}}{M} \tag{14}$$

where S symbolizes the specific surface area (m² g⁻¹); N_A signifies Avogadro’s number (6.02 × 10²³ mol⁻¹); q_{max} (mg g⁻¹) refers to the monolayer sorption capacity; a_{MB} implies the cross-sectional area of the MB = 120 Å²; and M denotes the molecular weight of MB. As is seen in Table 1, the GO/Ag nanocomposites

Table 4 Parameters of Langmuir, Freundlich, Temkin, and (D-R) isotherm models for various synthesized nanocomposites

Adsorption isotherms and their constants	The synthesized samples									
	GO/Ag-2	GO/Ag-6	GO/Ag-9	GO/Ag-18	GO/Ag(24R)-2	GO/Ag(24R)-18	GO(24R)-2	GO(24R)-18	GO	GO
Langmuir										
q_{\max} (mg g ⁻¹)	531.91	588.23	633.30	490.19	500.00	300.40	431.00	280.02	469.48	
k_L (L mg ⁻¹)	4.94	3.69	2.34	1.55	2.00	1.76	1.90	1.66	2.09	
R^2	0.9995	0.9998	0.9989	0.9994	0.9995	0.9993	0.9979	0.9985	0.9995	
Freundlich										
K_F (mg g ⁻¹)	378.6	395	396	251.2	289	247.7	270.5	131.1	288.5	
n	4.14	3.37	2.45	3.20	3.48	3.49	3.95	6.81	3.53	
R^2	0.9684	0.9259	0.9609	0.9229	0.9254	0.8999	0.9573	0.84712	0.9727	
Temkin										
B (J mol ⁻¹)	79.346	103.094	133.876	88.271	88.201	79.099	69.655	23.677	85.303	
k_T (L g ⁻¹)	159.0	59.5	23.9	21.9	33.8	29.2	66.1	242.3	38.0	
R^2	0.9749	0.9649	0.9825	0.9602	0.9640	0.9388	0.9627	0.838	0.9822	
(D-R isotherm)										
q_s (mg g ⁻¹)	470	498	558	438	484	400	375	199	424	
K_{DR} (mol ² kJ ⁻²)	0.07853	0.1220	0.5118	0.1600	0.0979	0.0579	0.103	0.0996	0.0514	
E (kJ mol ⁻¹)	2.523	2.024	0.9891	1.767	2.259	4.389	2.203	2.420	3.162	
R^2	0.9805	0.9744	0.9736	0.9726	0.9913	0.9979	0.9711	0.9850	0.9722	

Table 5 Comparison of the maximum adsorption capacity of different adsorbents towards the removal of MB

Adsorbents	q_{\max} (mg g ⁻¹)	References
Magnetic-modified multi-walled carbon nanotubes	48.08	(Madrakian et al. 2011)
Metal-organic frameworks/GO (MOFs/GO) composite	183.49	(Ling Li et al. 2013a)
Magnetic graphene-carbon nanotube composite	65.79	(Wang et al. 2014)
Ultrasonic surface modified chitin supported on sand (USM-chitin/sand)	51.80	(Dotto et al. 2015)
Mixed oxide of Ti and Si	162.96	(Pal et al. 2016)
Cross-linked chitosan/sepiolite composite	40.98	(Marrakchi et al. 2016)
Tetragonal ZrO ₂ -modified hematite mesoporous composite	44.70	(Sengupta et al. 2017)
RGO-Fe ₂ O ₃ -Fe ₃ O ₄ composite	75.00	(Saiphaneendra et al. 2017)
Fe ₃ O ₄ @ Ag/SiO ₂ nanospheres	128.50	(Saini et al. 2018)
Mesoporous activated carbon-alginate beads	230.00	(Nasrullah et al. 2018)
Manganese oxide embedded mesoporous carbon (MOPC950)	124.00	(Van Tran et al. 2019)
Polyaniline/reduced graphene oxide (PANI/RGO)	31.25	(El-Sharkaway et al. 2019)
Lignosulfonate/amino-functionalized SBA-15 composite	62.89	(Abboud et al. 2020)
PANI@TiO ₂ and PANI@SiO ₂ composites	89 and 74	(Maruthapandi et al. 2020)
rGO/Ag nanocomposite	300.40	This work
GO/Ag nanocomposites	490.19–633.30	This work

formed at room temperature such as GO/Ag-2, GO/Ag-6, GO/Ag-9, and GO/Ag-18 exhibited higher available areas for MB adsorption than those calculated for rGO/Ag nanocomposite as with GO/Ag(24R)-18.

In addition, our prepared GO showed a specific surface area of about $1060 \text{ m}^2 \text{ g}^{-1}$, which is very similar to the theoretical surface area of GO and is not so far from that measured using the UV-vis method based on surface coverage with MB (Montes-Navajas et al. 2013; Zhang et al. 2020). It should be noted that the area specified by the MB adsorption is larger than the values obtained by the BET model (Zhang et al. 2020). This is because nitrogen molecules penetrate very limitedly into the inner space of the dry solids (Hegyesi et al. 2017), also because drying induces the agglomeration of GO or GO-based nanomaterials (Zhang et al. 2020). GO is well known for being entirely exfoliated and homogeneously distributed in water. The drying process could, therefore, be barred if the actual surface area could be evaluated in water and GO samples prevented from agglomerating.

To affirm the strong potential of the nanocomposites (GO/Ag) as efficient adsorbents for removing MB from an aqueous solution, their adsorption ability was compared with different materials (Table 5). Their performance turned out to be higher than that of most late-use adsorbents. Although the rGO/Ag nanocomposite adsorption limit was lower than that reported for all GO/Ag nanocomposites, it also showed much greater viability than various adsorbents (Table 5).

Conclusion

The current study provides a feasible immobilization of green synthesized AgNPs on the nanosheets of GO and rGO by means of in situ reduction process using green tea aqueous extract as a reductant and stabilizer. Diverse techniques (XRD, FTIR, TGA, Raman, SEM, and TEM) have been used to identify the nanocomposites. Characterization findings have shown that AgNPs have been decorated on GO nanosheets where GO/Ag nanocomposites are feasibly formed at room temperature, even at low extract concentration (2%). Increasing extract concentrations from 6 to 18% results in higher yields of AgNPs on GO. While the formation of AgNPs on the rGO nanosheets (rGO/Ag nanocomposite) occurred only at a higher temperature (95 °C) in the presence of high extract concentration (18%). It should be noted that, contrary to chemical methods for

preparing rGO, the current study provides a safe alternative using green tea leaf extract (18%) at a temperature of 95 °C. The synthesized solid samples were used as eco-friendly adsorbents for extracting MB dye from the aqueous solution. The adsorption results indicate that GO/Ag-nanocomposites are highly capable of removing MB and displaying high adsorption potential of up to 633.3 mg g^{-1} . Adsorbent dose, initial MB concentration, pH, and contact time affect the adsorption process. The adsorption data was largely compatible with the Langmuir model. From the kinetic study, the adsorption process pursued a pseudo-second-order model. Thermodynamic parameters disclose the spontaneous adsorption process and its endothermic nature. Due to the excellent efficiency and recycling without releasing AgNPs, the synthesized nanocomposites can be used as effective eco-friendly adsorbents in wastewater treatment.

Acknowledgments The authors would like to thank the central lab of Tanta University for measuring XRD for the synthesized samples.

Compliance with ethical standards

Conflict of interest The authors declare that they have no conflict of interest.

References

- Abboud, M., Sahlabji, T., Haija, M. A., El-Zahhar, A. A., Bondock, S., Ismail, I., et al. (2020). Synthesis and characterization of lignosulfonate/amino-functionalized SBA-15 nanocomposites for the adsorption of methylene blue from wastewater. *New Journal of Chemistry*, 44(6), 2291–2302.
- Aboelfetoh, E. F., El-Shenody, R. A., & Ghobara, M. M. (2017). Eco-friendly synthesis of silver nanoparticles using green algae (*Caulerpa serrulata*): Reaction optimization, catalytic and antibacterial activities. *Environmental Monitoring and Assessment*, 189(7), 349.
- Aboelfetoh, E. F., Elhelaly, A. A., & Gemeay, A. H. (2018). Synergistic effect of Cu (II) in the one-pot synthesis of reduced graphene oxide (rGO/CuxO) nanohybrids as adsorbents for cationic and anionic dyes. *Journal of Environmental Chemical Engineering*, 6(1), 623–634.
- Aboubaraka, A. E., Aboelfetoh, E. F., & Ebeid, E.-Z. M. (2017). Coagulation effectiveness of graphene oxide for the removal of turbidity from raw surface water. *Chemosphere*, 181, 738–746.
- Agnihotri, S., Mukherji, S., & Mukherji, S. (2014). Size-controlled silver nanoparticles synthesized over the range 5–100 nm

- using the same protocol and their antibacterial efficacy. *RSC Advances*, 4(8), 3974–3983.
- Ahmadzadeh Tofighy, M., & Mohammadi, T. (2014). Methylene blue adsorption onto granular activated carbon prepared from Harmal seeds residue. *Desalination and Water Treatment*, 52(13–15), 2643–2653.
- Allen, H. J., Impellitteri, C. A., Macke, D. A., Heckman, J. L., Poynton, H. C., Lazorchak, J. M., Govindaswamy, S., Roose, D. L., & Nadagouda, M. N. (2010). Effects from filtration, capping agents, and presence/absence of food on the toxicity of silver nanoparticles to *Daphnia magna*. *Environmental Toxicology and Chemistry*, 29(12), 2742–2750.
- Beyene, H. D., Werkneh, A. A., Bezabh, H. K., & Ambaye, T. G. (2017). Synthesis paradigm and applications of silver nanoparticles (AgNPs), a review. *Sustainable Materials and Technologies*, 13, 18–23.
- Chieng, H. I., Priyantha, N., & Lim, L. B. (2015). Effective adsorption of toxic brilliant green from aqueous solution using peat of Brunei Darussalam: Isotherms, thermodynamics, kinetics and regeneration studies. *RSC Advances*, 5(44), 34603–34615.
- Chook, S. W., Chia, C. H., Zakaria, S., Ayob, M. K., Chee, K. L., Huang, N. M., et al. (2012). Antibacterial performance of Ag nanoparticles and AgGO nanocomposites prepared via rapid microwave-assisted synthesis method. *Nanoscale Research Letters*, 7(1), 1–7.
- de Moraes, A. C. M., Lima, B. A., de Faria, A. F., Brocchi, M., & Alves, O. L. (2015). Graphene oxide-silver nanocomposite as a promising biocidal agent against methicillin-resistant *Staphylococcus aureus*. *International Journal of Nanomedicine*, 10, 6847.
- Długosz, O., Chwastowski, J., & Banach, M. (2020). Hawthorn berries extract for the green synthesis of copper and silver nanoparticles. *Chemical Papers*, 74(1), 239–252.
- Dotto, G., dos Santos, J. N., Rosa, R., Pinto, L., Pavan, F., & Lima, E. (2015). Fixed bed adsorption of methylene blue by ultrasonic surface modified chitin supported on sand. *Chemical Engineering Research and Design*, 100, 302–310.
- Dubale, A. A., Su, W.-N., Tamirat, A. G., Pan, C.-J., Aragaw, B. A., Chen, H.-M., et al. (2014). The synergetic effect of graphene on Cu 2 O nanowire arrays as a highly efficient hydrogen evolution photocathode in water splitting. *Journal of Materials Chemistry A*, 2(43), 18383–18397.
- El-Sharkaway, E., Kamel, R. M., El-Sherbiny, I. M., & Gharib, S. S. (2019). Removal of methylene blue from aqueous solutions using polyaniline/graphene oxide or polyaniline/reduced graphene oxide composites. *Environmental Technology*, (just-accepted), 1–35.
- Ferrero, F. (2010). Adsorption of methylene blue on magnesium silicate: Kinetics, equilibria and comparison with other adsorbents. *Journal of Environmental Sciences*, 22(3), 467–473.
- Fujiki, H., Watanabe, T., Sueoka, E., Rawangkan, A., & Suganuma, M. (2018). Cancer prevention with green tea and its principal constituent, EGCG: From early investigations to current focus on human cancer stem cells. *Molecules and Cells*, 41(2), 73–82.
- Gao, J. J., Qin, Y. B., Zhou, T., Cao, D. D., Xu, P., Hochstetter, D., & Wang, Y. F. (2013). Adsorption of methylene blue onto activated carbon produced from tea (*Camellia sinensis* L.) seed shells: Kinetics, equilibrium, and thermodynamics studies. *Journal of Zhejiang University. Science. B*, 14(7), 650–658. <https://doi.org/10.1631/jzus.B12a0225>.
- Gemeay, A. H., Aboelfetoh, E. F., & El-Sharkawy, R. G. (2018a). Immobilization of green synthesized silver nanoparticles onto amino-functionalized silica and their application for indigo carmine dye removal. *Water, Air, & Soil Pollution*, 229(1), 16.
- Gemeay, A. H., Elsharkawy, R. G., & Aboelfetoh, E. F. (2018b). Graphene oxide/polyaniline/manganese oxide ternary nanocomposites, facile synthesis, characterization, and application for indigo carmine removal. *Journal of Polymers and the Environment*, 26(2), 655–669.
- Ghaedi, M., Sadeghian, B., Pebdani, A. A., Sahraei, R., Daneshfar, A., & Duran, C. (2012). Kinetics, thermodynamics and equilibrium evaluation of direct yellow 12 removal by adsorption onto silver nanoparticles loaded activated carbon. *Chemical Engineering Journal*, 187, 133–141.
- Haldorai, Y., Kim, B.-K., Jo, Y.-L., & Shim, J.-J. (2014). Ag@ graphene oxide nanocomposite as an efficient visible-light plasmonic photocatalyst for the degradation of organic pollutants: A facile green synthetic approach. *Materials Chemistry and Physics*, 143(3), 1452–1461.
- Haque, S., Gain, S., Gupta, K., & Ghosh, U. C. (2019). Methylene blue (a cationic dye) adsorption performance of graphene oxide fabricated Fe-Al bimetal oxide composite from water. *Water Quality Research Journal*, 54(1), 57–69.
- Hashemi, F., Tasharofi, N., & Saber, M. M. (2020). Green synthesis of silver nanoparticles using Teucrium polium leaf extract and assessment of their antitumor effects against MNK45 human gastric cancer cell line. *Journal of Molecular Structure*, 127889.
- Hebeish, A., El-Rafie, M., Abdel-Mohdy, F., Abdel-Halim, E., & Emam, H. E. (2010). Carboxymethyl cellulose for green synthesis and stabilization of silver nanoparticles. *Carbohydrate Polymers*, 82(3), 933–941.
- Hegyesi, N., Vad, R. T., & Pukánszky, B. (2017). Determination of the specific surface area of layered silicates by methylene blue adsorption: The role of structure, pH and layer charge. *Applied Clay Science*, 146, 50–55.
- Heidarizad, M., & Şengör, S. S. (2016). Synthesis of graphene oxide/magnesium oxide nanocomposites with high-rate adsorption of methylene blue. *Journal of Molecular Liquids*, 224, 607–617.
- Hou, C., Zhang, Q., Wang, H., & Li, Y. (2011). Functionalization of PNIPAAm microgels using magnetic graphene and their application in microreactors as switch materials. *Journal of Materials Chemistry*, 21(28), 10512–10517.
- Hou, I.-C., Amarnani, S., Chong, M. T., & Bishayee, A. (2013). Green tea and the risk of gastric cancer: Epidemiological evidence. *World Journal of Gastroenterology*, 19(24), 3713–3722.
- Huang, J., Zhang, L., Chen, B., Ji, N., Chen, F., Zhang, Y., & Zhang, Z. (2010). Nanocomposites of size-controlled gold nanoparticles and graphene oxide: Formation and applications in SERS and catalysis. *Nanoscale*, 2(12), 2733–2738.
- Huang, N., Lim, H., Chia, C. H., Yarmo, M. A., & Muhamad, M. (2011). Simple room-temperature preparation of high-yield large-area graphene oxide. *International Journal of Nanomedicine*, 6, 3443.

- Huang, L., Yang, H., Zhang, Y., & Xiao, W. (2016). Study on synthesis and antibacterial properties of Ag NPs/GO nanocomposites. *Journal of Nanomaterials*, 2016.
- Ismail, M. (2020). Green synthesis and characterizations of copper nanoparticles. *Materials Chemistry and Physics*, 240, 122283.
- Konicki, W., Aleksandrak, M., & Mijowska, E. (2017). Equilibrium, kinetic and thermodynamic studies on adsorption of cationic dyes from aqueous solutions using graphene oxide. *Chemical Engineering Research and Design*, 123, 35–49.
- Kooh, M. R. R., Lim, L. B., Lim, L. H., & Dahri, M. K. (2016). Separation of toxic rhodamine B from aqueous solution using an efficient low-cost material, *Azolla pinnata*, by adsorption method. *Environmental Monitoring and Assessment*, 188(2), 1–15.
- Kumar, S. V., Huang, N. M., Lim, H. N., Marlinda, A., Harrison, I., & Chia, C. H. (2013). One-step size-controlled synthesis of functional graphene oxide/silver nanocomposites at room temperature. *Chemical Engineering Journal*, 219, 217–224.
- Lee, S. H., & Jun, B.-H. (2019). Silver nanoparticles: Synthesis and application for nanomedicine. *International Journal of Molecular Sciences*, 20(4), 865.
- Lee, L.-S., Kim, S.-H., Kim, Y.-B., & Kim, Y.-C. (2014). Quantitative analysis of major constituents in green tea with different plucking periods and their antioxidant activity. *Molecules*, 19(7), 9173–9186.
- Li, L., Liu, X. L., Geng, H. Y., Hu, B., Song, G. W., & Xu, Z. S. (2013a). A MOF/graphite oxide hybrid (MOF: HKUST-1) material for the adsorption of methylene blue from aqueous solution. *Journal of Materials Chemistry A*, 1(35), 10292–10299.
- Li, Y., Du, Q., Liu, T., Sun, J., Wang, Y., Wu, S., et al. (2013b). Methylene blue adsorption on graphene oxide/calcium alginate composites. *Carbohydrate Polymers*, 95(1), 501–507.
- Lightcap, I. V., Kosel, T. H., & Kamat, P. V. (2010). Anchoring semiconductor and metal nanoparticles on a two-dimensional catalyst mat. Storing and shuttling electrons with reduced graphene oxide. *Nano Letters*, 10(2), 577–583.
- Liu, C.-C., Xu, H., Wang, L., & Qin, X. (2017). Facile one-pot green synthesis and antibacterial activities of GO/Ag nanocomposites. *Acta Metallurgica Sinica (English Letters)*, 30(1), 36–44.
- Madrakian, T., Afkhami, A., Ahmadi, M., & Bagheri, H. (2011). Removal of some cationic dyes from aqueous solutions using magnetic-modified multi-walled carbon nanotubes. *Journal of Hazardous Materials*, 196, 109–114.
- Mahmoud, M. E., Amira, M. F., Seleim, S. M., & Mohamed, A. K. (2017). Adsorption isotherm models, kinetics study, and thermodynamic parameters of Ni (II) and Zn (II) removal from water using the LbL technique. *Journal of Chemical & Engineering Data*, 62(2), 839–850.
- Marrakchi, F., Khanday, W., Asif, M., & Hameed, B. (2016). Cross-linked chitosan/sepiolite composite for the adsorption of methylene blue and reactive orange 16. *International Journal of Biological Macromolecules*, 93, 1231–1239.
- Martínez-Orozco, R., Rosu, H., Lee, S.-W., & Rodríguez-González, V. (2013). Understanding the adsorptive and photoactivity properties of Ag-graphene oxide nanocomposites. *Journal of Hazardous Materials*, 263, 52–60.
- Maruthapandi, M., Eswaran, L., Luong, J. H., & Gedanken, A. (2020). Sonochemical preparation of polyaniline@ TiO₂ and polyaniline@ SiO₂ for the removal of anionic and cationic dyes. *Ultrasonics Sonochemistry*, 62, 104864.
- Montes-Navajas, P., Asenjo, N. G., Santamaría, R., Menendez, R., Corma, A., & García, H. (2013). Surface area measurement of graphene oxide in aqueous solutions. *Langmuir*, 29(44), 13443–13448.
- Nasrullah, A., Bhat, A., Naeem, A., Isa, M. H., & Danish, M. (2018). High surface area mesoporous activated carbon-alginate beads for efficient removal of methylene blue. *International Journal of Biological Macromolecules*, 107, 1792–1799.
- Pal, U., Sandoval, A., Madrid, S. I. U., Corro, G., Sharma, V., & Mohanty, P. (2016). Mixed titanium, silicon, and aluminum oxide nanostructures as novel adsorbent for removal of rhodamine 6G and methylene blue as cationic dyes from aqueous solution. *Chemosphere*, 163, 142–152.
- Razzaque, S., Hussain, S. Z., Hussain, I., & Tan, B. (2016). Design and utility of metal/metal oxide nanoparticles mediated by thioether end-functionalized polymeric ligands. *Polymers*, 8(4), 156.
- Rolim, W. R., Pelegrino, M. T., de Araújo Lima, B., Ferraz, L. S., Costa, F. N., Bernardes, J. S., et al. (2019). Green tea extract mediated biogenic synthesis of silver nanoparticles: Characterization, cytotoxicity evaluation and antibacterial activity. *Applied Surface Science*, 463, 66–74.
- Rónavári, A., Kovács, D., Igaz, N., Vágvolgyi, C., Boros, I. M., Kónya, Z., et al. (2017). Biological activity of green-synthesized silver nanoparticles depends on the applied natural extracts: A comprehensive study. *International Journal of Nanomedicine*, 12, 871.
- Saini, J., Garg, V., & Gupta, R. (2018). Removal of methylene blue from aqueous solution by Fe₃O₄@ Ag/SiO₂ nanospheres: Synthesis, characterization and adsorption performance. *Journal of Molecular Liquids*, 250, 413–422.
- Saiphaneendra, B., Saxena, T., Singh, S. A., Madras, G., & Srivastava, C. (2017). Synergistic effect of co-existence of hematite (α-Fe₂O₃) and magnetite (Fe₃O₄) nanoparticles on graphene sheet for dye adsorption. *Journal of Environmental Chemical Engineering*, 5(1), 26–37.
- Salem, W., Leitner, D. R., Zingl, F. G., Schratte, G., Prassl, R., Goessler, W., et al. (2015). Antibacterial activity of silver and zinc nanoparticles against *Vibrio cholerae* and enterotoxigenic *Escherichia coli*. *International Journal of Medical Microbiology*, 305(1), 85–95.
- Sang, S., Li, D., Zhang, H., Sun, Y., Jian, A., Zhang, Q., et al. (2017). Facile synthesis of AgNPs on reduced graphene oxide for highly sensitive simultaneous detection of heavy metal ions. *RSC Advances*, 7(35), 21618–21624.
- Sengupta, A., Mallick, S., & Bahadur, D. (2017). Tetragonal nanostructured zirconia modified hematite mesoporous composite for efficient adsorption of toxic cations from wastewater. *Journal of Environmental Chemical Engineering*, 5(5), 5285–5292.
- Shao, Y., Wang, X., Kang, Y., Shu, Y., Sun, Q., & Li, L. (2014). Application of Mn/MCM-41 as an adsorbent to remove methyl blue from aqueous solution. *Journal of Colloid and Interface Science*, 429, 25–33.
- Shao, W., Liu, X., Min, H., Dong, G., Feng, Q., & Zuo, S. (2015). Preparation, characterization, and antibacterial activity of

- silver nanoparticle-decorated graphene oxide nanocomposite. *ACS Applied Materials & Interfaces*, 7(12), 6966–6973.
- Sharma, P., Hussain, N., Borah, D. J., & Das, M. R. (2013). Kinetics and adsorption behavior of the methyl blue at the graphene oxide/reduced graphene oxide nanosheet–water interface: A comparative study. *Journal of Chemical & Engineering Data*, 58(12), 3477–3488.
- Sobon, G., Sotor, J., Jagiello, J., Kozinski, R., Zdrojek, M., Holdynski, M., Paletko, P., Boguslawski, J., Lipinska, L., & Abramski, K. M. (2012). Graphene oxide vs. reduced graphene oxide as saturable absorbers for Er-doped passively mode-locked fiber laser. *Optics Express*, 20(17), 19463–19473.
- Sun, Q., Cai, X., Li, J., Zheng, M., Chen, Z., & Yu, C.-P. (2014). Green synthesis of silver nanoparticles using tea leaf extract and evaluation of their stability and antibacterial activity. *Colloids and Surfaces A: Physicochemical and Engineering Aspects*, 444, 226–231.
- Tang, X.-Z., Li, X., Cao, Z., Yang, J., Wang, H., Pu, X., et al. (2013). Synthesis of graphene decorated with silver nanoparticles by simultaneous reduction of graphene oxide and silver ions with glucose. *Carbon*, 59, 93–99.
- Van Tran, T., Nguyen, D. T. C., Le, H. T., Duong, C. D., Bach, L. G., Nguyen, H.-T. T., et al. (2019). Facile synthesis of manganese oxide-embedded mesoporous carbons and their adsorbability towards methylene blue. *Chemosphere*, 227, 455–461.
- Vi, T. T. T., Rajesh Kumar, S., Rout, B., Liu, C.-H., Wong, C.-B., Chang, C.-W., et al. (2018). The preparation of graphene oxide-silver nanocomposites: The effect of silver loads on gram-positive and gram-negative antibacterial activities. *Nanomaterials*, 8(3), 163.
- Vidhu, V., & Philip, D. (2014). Catalytic degradation of organic dyes using biosynthesized silver nanoparticles. *Micron*, 56, 54–62.
- Wang, P., Cao, M., Wang, C., Ao, Y., Hou, J., & Qian, J. (2014). Kinetics and thermodynamics of adsorption of methylene blue by a magnetic graphene-carbon nanotube composite. *Applied Surface Science*, 290, 116–124.
- Xiong, Z., Zhang, L. L., Ma, J., & Zhao, X. (2010). Photocatalytic degradation of dyes over graphene–gold nanocomposites under visible light irradiation. *Chemical Communications*, 46(33), 6099–6101.
- Yang, X., Li, Y., Du, Q., Wang, X., Hu, S., Chen, L., et al. (2016). Adsorption of methylene blue from aqueous solutions by polyvinyl alcohol/graphene oxide composites. *Journal of Nanoscience and Nanotechnology*, 16(2), 1775–1782.
- Zhang, S., Wang, H., Liu, J., & Bao, C. (2020). Measuring the specific surface area of monolayer graphene oxide in water. *Materials Letters*, 261, 127098.

Publisher's note Springer Nature remains neutral with regard to jurisdictional claims in published maps and institutional affiliations.